

# Generic Objective Vortices for Flow Visualization

TOBIAS GÜNTHER and MARKUS GROSS, ETH Zürich  
HOLGER THEISEL, University of Magdeburg

In flow visualization, vortex extraction is a long-standing and unsolved problem. For decades, scientists developed numerous definitions that characterize vortex regions and their corelines in different ways, but none emerged as ultimate solution. One reason is that almost all techniques have a fundamental weakness: they are not invariant under changes of the reference frame, i.e., they are not objective. This has two severe implications: First, the result depends on the movement of the observer, and second, they cannot track vortices that are moving on arbitrary paths, which limits their reliability and usefulness in practice. Objective measures are rare, but recently gained more attention in the literature. Instead of only introducing a new objective measure, we show in this paper how all existing measures that are based on velocity and its derivatives can be made objective. We achieve this by observing the vector field in optimal local reference frames, in which the temporal derivative of the flow vanishes, i.e., reference frames in which the flow appears steady. The central contribution of our paper is to show that these optimal local reference frames can be found by a simple and elegant linear optimization. We prove that in the optimal frame, all local vortex extraction methods that are based on velocity and its derivatives become objective. We demonstrate our approach with objective counterparts to  $\lambda_2$ , vorticity and Sujudi-Haines.

CCS Concepts: • Human-centered computing → Scientific visualization;

Additional Key Words and Phrases: Scientific visualization, vortex extraction, objectivity, optimal reference frame, linear optimization

## ACM Reference format:

Tobias Günther, Markus Gross, and Holger Theisel. 2017. Generic Objective Vortices for Flow Visualization. *ACM Trans. Graph.* 36, 4, Article 141 (July 2017), 11 pages.

DOI: <http://dx.doi.org/10.1145/3072959.3073684>

## 1 INTRODUCTION

Vortices are omnipresent features. Even though they have been studied for centuries, there is still no commonly agreed upon definition of what a vortex is. Scientists developed numerous definitions that characterize vortex regions and their corelines in different ways, but none emerged as ultimate solution. The definition of vortex concepts together with numerical methods to extract and visualize them is an active field of research not only in visualization but also in fluid dynamics, physics, and dynamical systems theory.

Most existing vortex concepts have a fundamental weakness: they are not invariant under changes of the reference frame. To illustrate this, consider Fig. 1. We see a simple 2D flow, e.g., a river. A person observing the flow from a helicopter that stands still (left) observes a different flow than a person in a helicopter that moves

Permission to make digital or hard copies of all or part of this work for personal or classroom use is granted without fee provided that copies are not made or distributed for profit or commercial advantage and that copies bear this notice and the full citation on the first page. Copyrights for components of this work owned by others than ACM must be honored. Abstracting with credit is permitted. To copy otherwise, or republish, to post on servers or to redistribute to lists, requires prior specific permission and/or a fee. Request permissions from [permissions@acm.org](mailto:permissions@acm.org).

© 2017 ACM. 0730-0301/2017/7-ART141 \$15.00  
DOI: <http://dx.doi.org/10.1145/3072959.3073684>

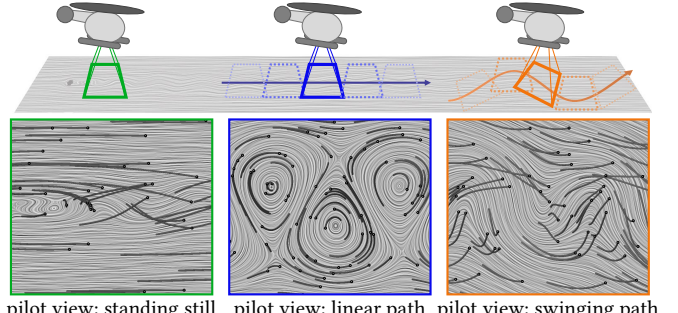


Fig. 1. Most flow visualization techniques depend on the movement of the observer, i.e., they are not objective. Here, a line integral convolution (time slice) and pathlines (black) are shown for three different reference frame movements: standing still, linearly translating and swinging along a sine curve—unfortunately, all give different results. We solve this ambiguity by finding an optimal local reference frame, in which the flow appears steady. In our optimal frame, all vortex extraction methods that are based on velocity and Jacobian become objective, including vorticity,  $\lambda_2$  and Sujudi-Haines.

with constant speed (middle). Figs. 1 (lower left) and (lower middle) show the flows as observed from the two helicopters, i.e., in different reference frames. A vortex concept that is invariant under such an equal-speed translation of the reference frame is called *Galilean invariant*. Fig. 1 (right) shows the observation of the flow under an arbitrary movement of the helicopter. A vortex measure that is invariant under such an arbitrarily moving reference frame is called *objective*. Objectivity is a highly desirable property, but most existing vortex concepts are only Galilean invariant; not objective.

The contribution of this paper is not just another objective vortex definition. Instead, we propose a generic method that transforms almost every existing vortex measure into an objective one. The main idea is to compute a local optimal reference frame for every point in the domain. Optimal means to have an observed velocity field that is as steady (i.e., time-independent) as possible in a small region around the point of interest. After showing that the locally optimal frame can be computed by a simple linear optimization at every point, we obtain new objective versions of the velocity, Jacobian and acceleration fields. Then, an existing vortex measure can be made objective simply by replacing the original fields with their objective counterparts. We cannot consider all new objective vortex measures that can be obtained by our method. For the evaluation, we restrict ourselves to the objective versions of common standard measures:  $\lambda_2$ , vorticity and Sujudi-Haines. We compare these with their original concepts and existing objective measures.

## Notation

Given is an  $n$ -dimensional ( $n = 2, 3$ ) time-dependent vector field  $\mathbf{v}(\mathbf{x}, t) = \mathbf{v}(x, y, [z], t)$ . The Jacobian matrix  $\mathbf{J} = (\frac{\partial \mathbf{v}}{\partial \mathbf{x}}, \frac{\partial \mathbf{v}}{\partial \mathbf{y}}, [\frac{\partial \mathbf{v}}{\partial z}])$  contains its spatial derivatives. We denote the temporal derivative as  $\mathbf{v}_t = \frac{\partial \mathbf{v}}{\partial t}$  and thus acceleration is  $\mathbf{a} = \mathbf{J}\mathbf{v} + \mathbf{v}_t$ . The Jacobian  $\mathbf{J}$  can be

decomposed into  $\mathbf{J} = \mathbf{S} + \boldsymbol{\Omega}$ , where  $\mathbf{S} = \frac{1}{2}(\mathbf{J} + \mathbf{J}^T)$  is the symmetric part and  $\boldsymbol{\Omega} = \frac{1}{2}(\mathbf{J} - \mathbf{J}^T)$  is the anti-symmetric part. We use function  $ap$  to transform the anti-symmetric part of a matrix to a scalar/vector. In 3D,  $ap(\mathbf{M}) = \frac{1}{2}(m_{3,2} - m_{2,3}, m_{1,3} - m_{3,1}, m_{2,1} - m_{1,2})^T$  and in 2D,  $ap(\mathbf{M}) = \frac{1}{2}(m_{1,2} - m_{2,1})$ , where  $m_{i,j}$  refer to the elements of the matrix  $\mathbf{M}$ . The inverse of  $ap$  is the function  $sk$  that transforms a scalar/vector into an antisymmetric matrix. In 2D and 3D, we have:

$$sk(\alpha) = \begin{pmatrix} 0 & \alpha \\ -\alpha & 0 \end{pmatrix}, \quad sk\begin{pmatrix} \alpha \\ \beta \\ \gamma \end{pmatrix} = \begin{pmatrix} 0 & -\gamma & \beta \\ \gamma & 0 & -\alpha \\ -\beta & \alpha & 0 \end{pmatrix} \quad (1)$$

With this, vorticity is defined in 2D and 3D as:

$$2D: \boldsymbol{\omega} = ap(\boldsymbol{\Omega}) \quad 3D: \boldsymbol{\omega} = ap(\boldsymbol{\Omega}) \quad (2)$$

Further, we denote the Parallel Vectors Operator [Peikert and Roth 1999] of two vector fields as  $\parallel$ , which returns curves along which two given vector fields are parallel.  $\mathbf{I}$  denotes the identity matrix.

## 2 OBJECTIVITY

In continuum mechanics, objectivity refers to the invariance of a measure under a change of the reference frame that transforms a point  $(\mathbf{x}, t)$  in space-time to a new point  $(\mathbf{x}^*, t^*)$  by

$$\mathbf{x}^* = \mathbf{Q}(t) \mathbf{x} + \mathbf{c}(t), \quad t^* = t - a \quad (3)$$

where  $\mathbf{Q} \in SO(3)$  is a rotation matrix,  $\mathbf{c}$  is a translation vector, and  $a$  is a constant. We assume  $\mathbf{Q}$ ,  $\mathbf{c}$  to be smooth functions of  $t$ . Then, objectivity can be formalized [Truesdell and Noll 1965]:

*Definition 2.1.* A scalar  $s$  is objective if it remains unchanged under any change of the reference frame as in Eq. (3). A vector  $\mathbf{r}$  is objective if Eq. (3) transforms it to  $\mathbf{r}^* = \mathbf{Q}(t) \mathbf{r}$ . A second-order tensor  $\mathbf{T}$  is objective if Eq. (3) transforms it to  $\mathbf{T}^* = \mathbf{Q}(t) \mathbf{T} \mathbf{Q}(t)^T$ .

A change of the reference frame using Eq. (3) transforms a velocity field and its derivatives into (for brevity we denote  $\mathbf{Q}(t)$  as  $\mathbf{Q}$ ):

$$\mathbf{v}^* = \mathbf{Q} \left( \mathbf{v} + \mathbf{Q}^T \dot{\mathbf{Q}} \mathbf{x} + \mathbf{Q}^T \dot{\mathbf{c}} \right) \quad (4)$$

$$\mathbf{J}^* = \mathbf{Q} \left( \mathbf{J} + \mathbf{Q}^T \ddot{\mathbf{Q}} \right) \mathbf{Q}^T \quad (5)$$

$$\mathbf{a}^* = \mathbf{Q} \left( \mathbf{a} + 2 \mathbf{Q}^T \dot{\mathbf{Q}} \mathbf{v} + \mathbf{Q}^T \ddot{\mathbf{Q}} \mathbf{x} + \mathbf{Q}^T \ddot{\mathbf{c}} \right) \quad (6)$$

$$\begin{aligned} \mathbf{v}_t^* = \mathbf{Q} & \left( \mathbf{v}_t - \mathbf{J} \mathbf{Q}^T \dot{\mathbf{Q}} \mathbf{x} + \mathbf{Q}^T \dot{\mathbf{Q}} \mathbf{v} - \mathbf{J} \mathbf{Q}^T \dot{\mathbf{c}} \right. \\ & \left. + (\mathbf{Q}^T \ddot{\mathbf{Q}} - (\mathbf{Q}^T \dot{\mathbf{Q}})^2) \mathbf{x} + (\mathbf{Q}^T \ddot{\mathbf{c}} - \mathbf{Q}^T \dot{\mathbf{Q}} \mathbf{Q}^T \dot{\mathbf{c}}) \right) \end{aligned} \quad (7)$$

$$\boldsymbol{\Omega}^* = \mathbf{Q} \left( \boldsymbol{\Omega} + \mathbf{Q}^T \dot{\mathbf{Q}} \right) \mathbf{Q}^T \quad \mathbf{S}^* = \mathbf{Q} \mathbf{S} \mathbf{Q}^T \quad (8)$$

$$\boldsymbol{\omega}^* = \mathbf{Q} \left( \boldsymbol{\omega} + ap(\mathbf{Q}^T \dot{\mathbf{Q}}) \right) \quad (9)$$

where  $\dot{\mathbf{Q}} = \frac{d\mathbf{Q}}{dt}$ ,  $\ddot{\mathbf{Q}} = \frac{d\dot{\mathbf{Q}}}{dt}$ ,  $\dot{\mathbf{c}} = \frac{d\mathbf{c}}{dt}$ ,  $\ddot{\mathbf{c}} = \frac{d\dot{\mathbf{c}}}{dt}$  are the time derivatives of  $\mathbf{Q}$  and  $\mathbf{c}$ . The proof of Eqs. (4)–(9) is in Appendix A. Eqs. (4)–(9) show that  $\mathbf{v}, \mathbf{v}_t, \mathbf{J}, \mathbf{a}, \boldsymbol{\Omega}, \boldsymbol{\omega}$  are not objective, as they do not obey Definition 2.1. Matrix  $\mathbf{S}$ , however, is objective.

The definition of objectivity requires that a measure is invariant under *global* rotations and translations of the observer. A global transformation, however, cannot adapt to the motion of vortices everywhere [Perry and Chong 1994], as they might move in different directions with different speeds. Instead, we search for transformations *locally*. In this local search, every global rotation and

translation of the observer is equally removed at each point, thus any global rotation and translation has no impact on the result. In this sense, our method becomes objective by the standard definition.

## 3 RELATED WORK

In this section, we explain the most commonly-used vortex measures. We note that dozens of other vortex extraction methods have been proposed, and we cannot hope to cover them all. We refer to [Günther et al. 2016; Laramee et al. 2007; Peikert and Roth 1999; Post et al. 2003] for a comprehensive introduction.

### 3.1 Galilean Invariant Measures

Among the region-based methods, Jeong and Hussain [1995] introduced the  $\lambda_2$  criterion, which identifies vortices as regions in which the second-largest eigenvalue of  $\mathbf{S}^2 + \boldsymbol{\Omega}^2$  is negative, i.e.,  $\lambda_2(\mathbf{S}^2 + \boldsymbol{\Omega}^2) < 0$ . Okubo [1970] and Weiss [1991] independently developed a criterion related to the  $Q$ -criterion of Hunt [1987].

Coreline extraction searches lines that particles rotate around. Sujudi and Haimes [1995] formulated the reduced vorticity criterion:  $\mathbf{v} - (\mathbf{v}^T \mathbf{e}) \mathbf{e} = \mathbf{0}$ , where  $\mathbf{e}$  is the eigenvector of  $\mathbf{J}$ , corresponding to the only real-valued eigenvalue. Peikert and Roth [1999] used the parallel vectors operator  $\parallel$  to rephrase this as  $\mathbf{v} \parallel \mathbf{J} \mathbf{v}$ , which avoids explicit computation of the eigenvectors. Note that these methods are not Galilean invariant in 3D. A Galilean invariant method was presented by Weinkauf et al. [2007], who extended the reduced vorticity criterion of Sujudi and Haimes [1995] to unsteady flows as:

$$2D: \mathbf{v} - \mathbf{f} = \mathbf{0} \quad 3D: \mathbf{J}(\mathbf{v} - \mathbf{f}) \parallel \mathbf{v} - \mathbf{f} \quad (10)$$

where  $\mathbf{f} = -\mathbf{J}^{-1} \mathbf{v}_t$  is the feature flow field [Theisel and Seidel 2003], cf. [Günther et al. 2016]. Roth and Peikert [1998] presented a higher-order method and Kasten et al. [2011a; 2011b] identified vortex cores by  $\mathbf{a} = \mathbf{0}$ , which is in 2D identical to Eq. (10). A 3D extension followed recently [Kasten et al. 2016]. Sahner et al. [2005] extracted extremum lines of region-based methods, which was followed by Schafhitzel et al. [2008], who considered the topology of  $\lambda_2$ -based vortex corelines. Later, Sahner et al. [2007] computed vortex and strain skeletons. Günther et al. [2016] proposed an approach to make Galilean invariant methods rotation invariant. Recently, Bujack et al. [2016] analyzed the extrema of the determinant of  $\mathbf{J}$ .

### 3.2 Objective Measures

*Relative Vorticity Tensor-based Measures.* While strain rate tensor  $\mathbf{S}$  is objective, cf. Eq. (8), vorticity tensor  $\boldsymbol{\Omega}$  is only Galilean invariant. To obtain an objective vorticity tensor, Drouot and Lucius [1976] built the *relative vorticity tensor*  $\tilde{\boldsymbol{\Omega}}$ , which views vorticity in strain basis:

$$\tilde{\boldsymbol{\Omega}} = \boldsymbol{\Omega} - \mathbf{W} \quad (11)$$

Thereby, the rate-of-rotation tensor  $\mathbf{W}$  is given by:  $D\mathbf{e}_i/Dt = \mathbf{W} \mathbf{e}_i$ , with  $\mathbf{e}_i$  being the unit eigenvectors of  $\mathbf{S}$  and  $D/Dt$  being the material derivative. The tensor  $\tilde{\boldsymbol{\Omega}}$  was independently identified by Tabor and Klapper [1994], who called it *effective rotation*. Astarita [1979] proved the objectivity of Eq. (11) and proposed an index that classifies the domain into extension-like motions and rigid-body-like rotations. When substituting the vorticity tensor  $\boldsymbol{\Omega}$  by the relative vorticity

tensor  $\tilde{\Omega}$ , traditional region-based methods can be made objective. An objective counterpart to  $\lambda_2$  is, cf. Martins et al. [2016]:

$$\lambda_2(S^2 + \tilde{\Omega}^2) < 0 \quad (12)$$

An objective counterpart to the Q criterion is, cf. Haller [2005]:  $[\tilde{\Omega}^2 - S^2]/2 > 0$ . We refer to Thompson [2008] for a fluid mechanics perspective on recent advances in this area.

*Strain Tensor-based Measures.* Haller [2005] proposed the  $M_z$  criterion, which defines a vortex as a set of fluid trajectories along which the strain acceleration tensor is indefinite over directions of zero strain. He computed a binary field that indicates whether the tensor is indefinite, which in turn marks non-hyperbolic particle behavior. Along particle trajectories, the binary value is averaged to find trajectories that stay in indefinite areas for a long time, assuming that long-term non-hyperbolic behavior is an indicator for a vortex. Sahner et al. [2007] extracted strain skeletons and extremal lines of  $M_z$ . In recent years, Lagrangian Coherent Structures (LCS) [Haller 2015] have been computed objectively using calculus of variations. LCSs are distinguished material curves that organize the flow. A subclass are elliptic LCS, which preserve arc length and area in incompressible 2D flows. Haller [2015] considered the outermost elliptic LCS, of a family of nested elliptic LCSs, as the boundary of a coherent vortex. Serra and Haller [2016b] used the variational framework to find objective Eulerian vortex boundaries as closed instantaneous (per time step) curves across which the averaged material stretching rate shows no leading-order variability. Based on these (instantaneous) curves, they forecasted the Lagrangian persistence of a vortex [Serra and Haller 2016a].

*Vorticity-based Measures.* Some objective measures were derived from vorticity. Note that vorticity itself is not objective, see Eq. (9). Haller et al. [2016] noted that any subtraction of two vorticity values  $\omega(x_1, t) - \omega(x_2, t)$  will cancel out the spatially-constant rotation rate  $ap(Q^T \dot{Q})$  of the reference frame, if the vorticity was sampled at the same time  $t$ . This means, every subtraction of two vorticity values is objective—including spatial derivatives. In 2D and 3D, Haller et al. [2016] subtracted the spatial mean of vorticity in a local neighborhood  $U \subseteq D$  to define instantaneous vorticity deviation (IVD). An extension is the Lagrangian-averaged vorticity deviation (LAVD), for which IVD is integrated along pathlines. Both IVD and LAVD are objective, cf. Haller et al. [2016], but the measures are *relative* to their neighborhood and thus their value-range depends on the neighborhood size. Even though these vorticity-based measures are gracefully objective (including the location of extrema), vorticity does not respond to irrotational vortices and produces false-positives in shear flow. Further, Lugt [1979] noted that a local vorticity extremum is not necessary for the existence of a vortex.

### 3.3 Vector Field Decomposition

Suitable reference frames were searched by subtraction of a mean flow or by a decomposition to remove a harmonic component. Bhatia et al. [2013] used the Helmholtz-Hodge decomposition (HDD) of a flow into divergence-free, irrotational and harmonic parts to extract vortices [Bhatia et al. 2014]. Note that a harmonic part cannot capture rotational transport, as it is always irrotational. Aside from using the HDD to change the reference frame, vortices have been

identified as extremal structures of the magnitude of the divergence-free part [Tong et al. 2003]. Unlike previous methods, we optimize for the reference frame in which the flow appears steady. Lugt [1979] noted that in unsteady flows there is no *global* distinguished reference frame in which the entire flow appears steady. Perry and Chong [1994] noted that in certain flows, e.g., jets in cross-flow, vortices move with different speed and thus become steady—and therefore visible—in different reference frames. In order to reveal the vortices everywhere, we do not seek for a global (spatially-constant) reference frame, but for *local* ones.

## 4 OBJECTIVITY BY OPTIMAL REFERENCE FRAME

The main idea of our approach is to estimate an optimal reference frame *locally* for every point  $(x, t)$ : the local frame  $(Q, c)$  is chosen such that the transformed velocity field is as steady as possible in a neighborhood of  $(x, t)$ . We locally assume that  $Q$  and  $c$  are spatially-constant. Since we waive the spatial and temporal connection to neighboring points, all derivatives are solved for individually, including  $\dot{Q}, \ddot{Q}, \dot{c}, \ddot{c}$ <sup>1</sup>. For every point  $(x, t)$ , we define a spatial neighborhood  $U$  around it to which we fit the reference frame transformation. To compute the optimal reference frame in  $U$ , we set  $Q = I, c = 0$ <sup>2</sup>, and find the unknowns  $\dot{Q}, \ddot{Q}, \dot{c}, \ddot{c}$ , which contain 6 scalars (angles and offsets) in 2D and 12 in 3D, that minimize

$$\int_U \|v_t^*\|^2 dV \rightarrow \min. \quad (13)$$

With these locally optimal  $\dot{Q}, \ddot{Q}, \dot{c}, \ddot{c}$ , we obtain the new local optimal fields  $\bar{v}, \bar{J}, \bar{v}_t, \bar{a}$  by applying Eqs. (4)–(7). With these, existing vortex measures can be made objective simply by replacing  $v, J, v_t, a$  with  $\bar{v}, \bar{J}, \bar{v}_t, \bar{a}$ , respectively. Note that although Eq. (13) is minimized for every point  $(x, t)$ , in practice it is computed only at discrete grid points; usually the same grid on which  $v$  is given.

Minimizing Eq. (13) is not straightforward, since  $v_t^*$  is non-linear in  $\dot{Q}, \ddot{Q}, \dot{c}, \ddot{c}$ . However,  $v_t^*$  can be equivalently rephrased and thereby *linearized* by substitution. Instead of solving for  $\dot{Q}, \ddot{Q}, \dot{c}, \ddot{c}$  directly<sup>3</sup>, we solve for a suitable combination of these unknowns, stored in  $u$ :

$$v_t^* = Q(v_t - M u). \quad (14)$$

In 3D,  $M$  is a  $3 \times 12$  matrix

$$M = (-J X + V, J, X, I) \quad (15)$$

with  $X = sk(x)$ ,  $V = sk(v)$ , and  $u$  is a 12-vector

$$u = \begin{pmatrix} u_1 \\ u_2 \\ u_3 \\ u_4 \end{pmatrix} = \begin{pmatrix} ap(Q^T \dot{Q}) \\ Q^T \dot{c} \\ ap(Q^T \ddot{Q} - (Q^T \dot{Q})^2) \\ -(Q^T \ddot{c} - Q^T \dot{Q} Q^T \dot{c}) \end{pmatrix}. \quad (16)$$

In 2D,  $M$  and  $u$  have a slightly different form.  $M$  is a  $2 \times 6$  matrix

$$M = (-J x_p + v_p, J, x_p, I) \quad (17)$$

<sup>1</sup> The temporal derivatives of  $Q$  cannot be computed by finite differences from adjacent time slices, since each point solves for the optimal frame independent of its neighbors. We explicitly compute  $\dot{Q}, \ddot{Q}$  at each point.

<sup>2</sup> Not prescribing  $Q$  and  $c$  results in a family of minimizers. By setting  $Q = I, c = 0$ , we select the solution that is located at  $x$ . The other solutions would be transformed by  $Q, c$  and are not objective, see Appendix B.

<sup>3</sup> With  $Q = I$ , it is possible to extract  $\dot{Q}, \ddot{Q}, \dot{c}, \ddot{c}$  from  $u_1, u_2, u_3, u_4$ .

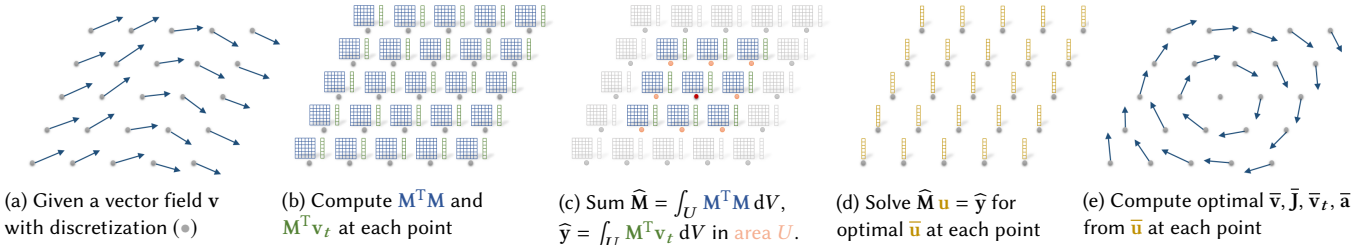


Fig. 2. Overview of our optimal reference frame computation. (a): Given is a vector field  $v$  with a discretization (•). (b): For each point, we compute  $M^T M$  and  $M^T v_t$  in a certain area  $U$  (here,  $3 \times 3$  voxels) to obtain  $\hat{M}$  and  $\hat{y}$  according to Eq. (19). (d): Given  $\hat{M}$  and  $\hat{y}$  at each point, we solve for the optimal vector  $\bar{u}$  in Eq. (18), which contains the parameters of the optimal reference frame. (e): Finally, we use  $\bar{u}$  to compute vector field  $\bar{v}$  and its derivatives  $\bar{J}, \bar{v}_t$  and  $\bar{a}$  in the optimal reference frame, see Eqs. (20)–(23).

with  $x_p = (-y, x)^T$ ,  $v_p = (-v, u)^T$ , and  $u$  is a 6-vector. Note that  $u_1$  and  $u_3$  are scalars in 2D, namely the first-order and second-order derivative of the angular velocity of the rotation of the frame. The reformulation of Eq. (7) into Eq. (14)–(17) is a straightforward exercise in algebra. Eq. (14) shows that the vector field and the reference frame are completely separated:  $M$  contains only  $v$  and its derivatives, while all information of the frame is stored in  $u$ .

Eq. (13) is minimized using Eq. (14), which can be written as the solution of the linear system

$$\hat{M} \bar{u} = \hat{y} \quad (18)$$

$$\text{with } \hat{M} = \int_U M^T M dV, \quad \hat{y} = \int_U M^T v_t dV. \quad (19)$$

Let  $\bar{u} = (\bar{u}_1, \bar{u}_2, \bar{u}_3, \bar{u}_4)^T = \hat{M}^{-1} \hat{y}$  be the solution of Eq. (18). Then, the new fields in the locally optimal reference frame are<sup>4</sup>

$$\bar{v} = v + sk(\bar{u}_1) x + \bar{u}_2 \quad (20)$$

$$\bar{J} = J + sk(\bar{u}_1) \quad (21)$$

$$\bar{v}_t = v_t - M \bar{u} \quad (22)$$

$$\bar{a} = \bar{J} \bar{v} + \bar{v}_t. \quad (23)$$

which follows directly from insertion of  $\bar{u}_1, \bar{u}_2, \bar{u}_3, \bar{u}_4$  into the Eqs. (4)–(7), using the operator  $sk$  from Eq. (1) to remove *ap*.

**THEOREM 4.1 (OBJECTIVITY IN OPTIMAL FRAMES).** *Given an at least  $C^1$  continuous vector field  $v$ , let  $\bar{v}$  be its observation in the most-steady reference frame and let  $\bar{J}, \bar{v}_t, \bar{a}$  be its observed derivatives. Any scalar measure  $s$  that is computed from  $\bar{v}, \bar{J}, \bar{a}, \bar{v}_t$  remains unchanged under any smooth rotation and translation of the reference frame of  $v$  as in Eq. (3). A vector  $r$  that is computed in the optimal frame from  $\bar{v}, \bar{J}, \bar{a}, \bar{v}_t$  is objective, i.e., a transformation of  $v$  via Eq. (3) transforms  $r$  to  $r^* = Q(t) r$ . A second-order tensor  $T$  computed from  $\bar{v}, \bar{J}, \bar{a}, \bar{v}_t$  is objective, since a transformation of  $v$  via Eq. (3) transforms  $T$  to  $T^* = Q(t) T Q(t)^T$ .*

See Appendix B for a proof that  $\bar{v}, \bar{J}, \bar{v}_t, \bar{a}$  are objective.

**THEOREM 4.2 (CONTINUITY OF SOLUTION).** *If the input vector field  $v$  is  $C^1$  continuous, then  $\bar{v}, \bar{J}, \bar{a}, \bar{v}_t$  are at least  $C^0$  continuous.*

All  $\bar{v}, \bar{J}, \bar{a}, \bar{v}_t$  are computed by integrating only first-order derivatives in a region  $U$ . If both  $v$  and its first-order partials are continuous (i.e.,  $v$  is  $C^1$  continuous), then  $\bar{v}$  is at least  $C^0$  continuous.

<sup>4</sup> Similar to the temporal derivatives of  $Q$ , spatial/temporal derivatives of  $\bar{v}$  cannot be computed by finite differences. Thus, we give explicit formulas.

## 5 VORTICES IN AN OPTIMAL REFERENCE FRAME

Using the optimal vector field  $\bar{v}$  and its derivatives  $\bar{J}, \bar{v}_t, \bar{a}$ , we can apply existing vortex extraction methods. Any useful vortex measure that is based on velocity and Jacobian can be made objective this way, as demonstrated next for selected well-established methods.

### 5.1 Line-based Vortex Measures

A necessary condition for vortices is the presence of complex eigenvalues in the Jacobian  $\bar{J}$ , as this indicates swirling motion. In 2D, objective vortex corelines appear as paths of critical points in  $\bar{v}$  and in 3D, objective vortex corelines are extracted by parallel vectors:

$$2D: \bar{v} = 0 \quad 3D: \bar{J} \bar{v} \parallel \bar{v}. \quad (24)$$

Note that these techniques usually only work in steady flows. Since we observe unsteady flows in the optimal near-steady reference frame, our method extracts vortex corelines of pathlines.

### 5.2 Region-based Vortex Measures

We propose a new objective vorticity tensor  $\bar{\Omega}$  that views vorticity in the optimal frame and use it to define a new objective  $\bar{\lambda}_2$  measure:

$$\bar{\lambda}_2(S^2 + \bar{\Omega}^2) < 0 \quad \text{with} \quad \bar{\Omega} = \frac{\bar{J} - \bar{J}^T}{2}. \quad (25)$$

We define an objective counterpart to the 2D and 3D vorticity as:

$$2D: \bar{\omega} = ap(\bar{J}) \quad 3D: \bar{\omega} = ap(\bar{J}). \quad (26)$$

## 6 IMPLEMENTATION

Our method can be seen as a pre-process, which fits well into existing visualization pipelines. We take a vector field as input and output the vector field and its derivatives in the optimal reference frame. The computation of the optimal reference frame is simple, local, easily parallelized and consists of five steps, as illustrated in Fig. 2.

- (1) **Discretization.** On simulated and measured flows, we use the discretization that is provided by the data. For analytic flows, we subdivide the domain uniformly. We used 2–8 million voxels, depending on the extent of the domain.
- (2) **Compute  $M^T M$  and  $M^T v_t$ .** For each grid point, we compute matrix  $M$  per Eqs. (15) and (17). Afterwards, we compute and store for every grid point  $M^T M$  and  $M^T v_t$ .
- (3) **Integrate Neighborhood  $U$ .** Around each point, we sum up  $M^T M$  and  $M^T v_t$  in a neighborhood  $U$  to obtain  $\hat{M}$  and  $\hat{y}$ , cf. Eq. (19). For regular grids, this is achieved per grid point

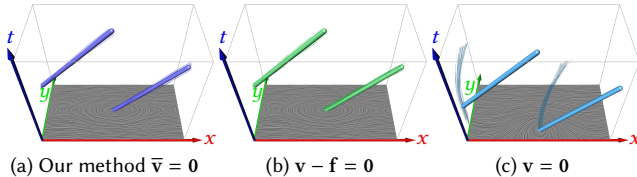


Fig. 3. STUART VORTEX. Our method (a) and the Galilean invariant method of Weinkauf et al. [2007] (b) are correct. Pathlines (thin) swirl away from streamline cores (thick) in (c), indicating that these are not rotation centers.

- in constant time with summed-area tables (also known as integral images), which are built in-place and in linear time.
- (4) **Solve  $\widehat{\mathbf{M}} \mathbf{u} = \widehat{\mathbf{y}}$ .** For each grid point, we solve the linear system in Eq. (18) to get reference frame parameters  $\bar{\mathbf{u}}$ . We use a Householder QR decomposition with full-pivoting.
  - (5) **Compute  $\bar{\mathbf{v}}, \bar{\mathbf{J}}, \bar{\mathbf{v}_t}, \bar{\mathbf{a}}$ .** Given the optimal parameters  $\bar{\mathbf{u}}$ , we compute and store the vector field and its derivatives in the optimal frame, see Eqs. (20)–(23).

Afterwards, we perform objective vortex extraction by applying standard techniques, as described in Section 5.

## 7 RESULTS

In the following, we start with simple reference frame movements in analytic flows and then move on to numerical simulations.

### 7.1 Special Case: Galilean invariance

Since our method is objective, it is necessarily Galilean invariant. We show this with a STUART VORTEX, which was frequently used to demonstrate Galilean invariance [Günther and Theisel 2014; Kasten et al. 2016; Weinkauf et al. 2007]. In a frame that translates with  $\mathbf{c} = (c t, 0)^T$ , cf. Eq. (4), the observed vector field is:

$$\mathbf{v}^*(x, y, t) = \begin{pmatrix} \frac{4 \sinh(y) + 4c \cosh(y) - c \cos(x - c t)}{4 \cosh(y) - \cos(x - c t)} \\ -\frac{\sin(x - c t)}{4 \cosh(y) - \cos(x - c t)} \end{pmatrix} \quad (27)$$

In the following, we set  $c = 1$  and observe the spatial domain  $D = [-4, 4] \times [-2, 2]$  with time  $T = [0, 2\pi]$ . Fig. 3 demonstrates a number of coreline extraction techniques that are based on critical point search in a certain vector field that is depicted as a LIC slice. Our method in Fig. 3a and the Galilean method of Weinkauf et al. [2007] in Fig. 3b produce identical results as expected. Extracting and connecting critical points in  $\mathbf{v}$  per time step in Fig. 3c, as done by Bauer and Peikert [2002], and Theisel et al. [2005], produces the cores of streamlines rather than pathlines.

### 7.2 Special Case: Rotation invariance

Objectivity also entails rotation invariance. We use the steady FOUR CENTERS vector field from Günther et al. [2016], which is defined in the domain  $D = [-2, 2]^2$ :

$$\mathbf{v}(x, y) = \begin{pmatrix} -x(2y^2 - 1)e^{-x^2 - y^2} \\ y(2x^2 - 1)e^{-x^2 - y^2} \end{pmatrix} \quad (28)$$

It contains two CW-rotating vortices at  $(\pm 2^{-1/2}, \pm 2^{-1/2})$  and two CCW-rotating vortices at  $(\pm 2^{-1/2}, \mp 2^{-1/2})$ . We observe the flow for time  $T = [0, 2\pi]$  in a reference frame that rotates CCW with

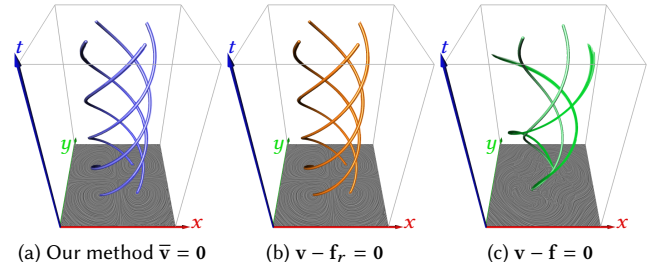


Fig. 4. FOUR CENTERS flow. Ideally, pathlines (thin), seeded at  $t = 0$ , should stay close to corelines (thick). Our method (a) and rotation invariance (b) give the same correct result. Galilean invariance (c) produces different corelines and pathlines drift away, indicating that these are not rotation centers.

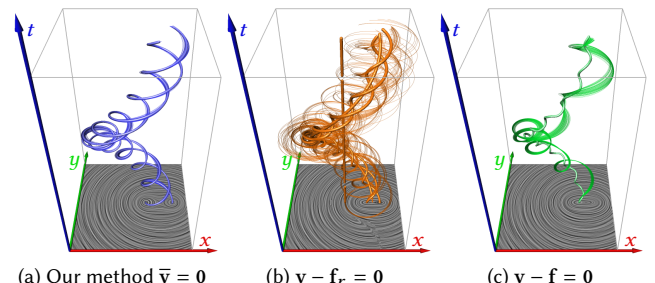


Fig. 5. HELIX flow. Our method (a) finds the ground truth, whereas rotation invariance (b) and Galilean invariance (c) do not detect the correct corelines. Pathlines (thin) were seeded at  $t = 0$  and stay at corelines (thick) in (a).

unit speed around the origin  $\mathbf{x}_0 = 0$ . Given the rotation center  $\mathbf{x}_0$ , the correct corelines are found with the rotation invariant method of Günther et al. [2016]. Our method finds the correct corelines, as well, demonstrating that rotation invariance is a special case, see Figs. 4a and 4b. A central advantage of our method over the rotation invariant approach [Günther et al. 2016] is that ours does not require the rotation center  $\mathbf{x}_0$  as input, i.e.,  $\mathbf{x}_0$  can be unknown. In comparison, Galilean invariance in Fig. 4c is not enough, since the vortices are not moving with equal speed on straight paths.

### 7.3 Non-linear Helix Movement

To show the need for objectivity, we construct an analytic flow, in which two vortices move on neither linear nor circular paths. Instead, they spiral around each other as they rotate around a common center. The flow is constructed by transforming the steady flow:

$$\mathbf{v}(x, y) = \frac{5}{2} \begin{pmatrix} -y(4y^2 + 4x^2 + 1) \\ x(4y^2 + 4x^2 - 1) \end{pmatrix} \quad (29)$$

with the transformation  $\begin{pmatrix} \cos(6t) & -\sin(6t) \\ \sin(6t) & \cos(6t) \end{pmatrix} \mathbf{x} + \begin{pmatrix} \cos(t) \\ \sin(t) \end{pmatrix}$  in the domain  $D = [-2, 2]^2$  with time  $T = [0, 2\pi]$ . Our objective method in Fig. 5a is able to detect the two ground truth corelines:  $\mathbf{y}_{\pm}(t) = (\cos(t), \sin(t))^T \pm (\cos(6t), \sin(6t))^T$ . Rotation invariance in Fig. 5b and Galilean invariance in Fig. 5c, however, give incorrect results.

### 7.4 Objective Corelines in Numerical 2D Flows

Next, we apply our technique to two numerical 2D simulations that were computed with Gerris Flow solver [Popinet 2004]. The 2D

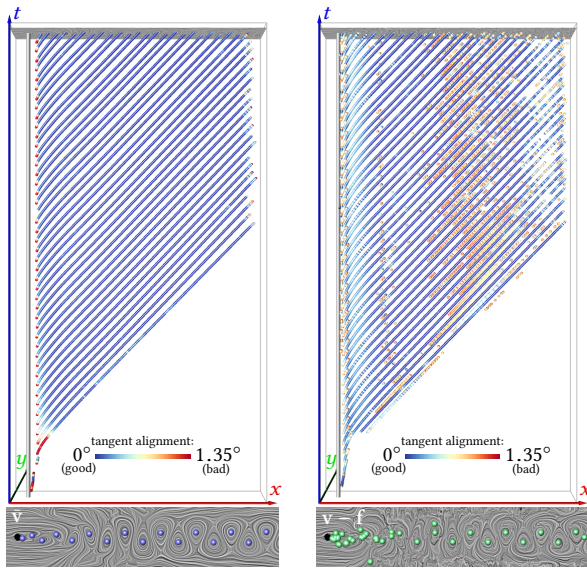


Fig. 6. The 2D CYLINDER flow is a prime test case for Galilean invariance. Our method (a) extracts corelines far more robustly than the Galilean invariant method of Weinkauf et al. [2007] in (b). Top: color denotes the angle between coreline tangent and the vector field. Bottom: LIC displays a time slice of the vector fields in which the critical points were extracted.

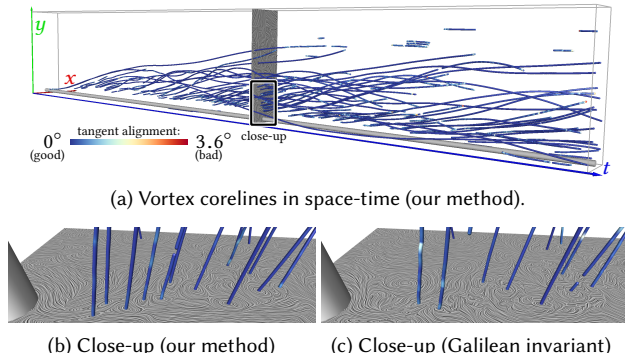
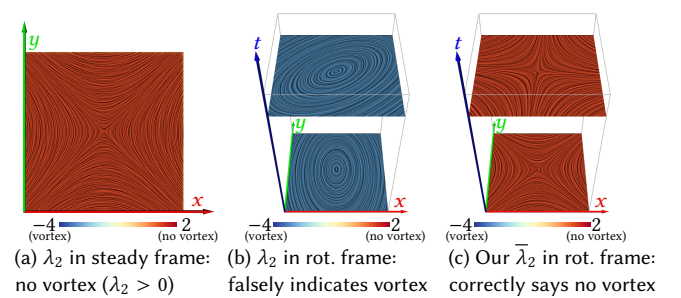
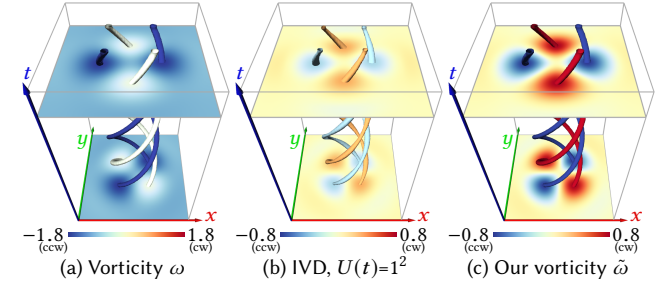


Fig. 7. BOUSSINESQ. Our corelines shown in space-time (a). Our method (b) extracts vortices behind the obstacle better than Weinkauf et al. [2007] (c).

CYLINDER flow contains a von-Kármán vortex street, i.e., a periodic shedding of vortices in the wake of an obstacle. The flow moves in from the left with a Reynolds number of  $Re = 160$ . Since vortices move with almost equal speed (except directly behind the obstacle) in an almost constant direction, the assumption of Galilean invariance is sufficient and should produce good results. To show that our method is at least as good as Galilean invariant approaches, we apply our objective coreline extraction and the Galilean invariant method of Weinkauf et al. [2007] in Fig. 6. We color-code the tangent alignment [Günther et al. 2016], which measures the angle between coreline tangent and pathline tangent in space-time, since ideally, corelines should follow pathlines. As shown in Fig. 6a for a window  $U$  that is 4× the radius of the obstacle, our method extracts the vortex cores far more robustly than Weinkauf et al. [2007] in



(a)  $\lambda_2$  in steady frame: (b)  $\lambda_2$  in rot. frame: (c) Our  $\tilde{\lambda}_2$  in rot. frame:  
no vortex ( $\lambda_2 > 0$ ) falsely indicates vortex correctly says no vortex  
Fig. 8. Consider a steady saddle flow (a). With a sufficiently fast rotation of the observer, the flow incorrectly appears to contain a vortex (b). In our optimal reference frame, the rotation is removed (c), showing correctly that no vortex is present. In all images, LIC shows the flow and  $\lambda_2$  is color-coded.



(a) Vorticity  $\omega$  (b) IVD,  $U(t)=t^2$  (c) Our vorticity  $\tilde{\omega}$   
Fig. 9. Vorticity in FOUR CENTERS flow. With original vorticity (a) all vortices appear to rotate CCW. With IVD (b) the magnitude (apparent vortex strength) depends on the neighborhood  $U$ . With our method (c) the rotation is removed and the vorticity magnitude is the same as in the steady frame.

Fig. 6b. The latter requires manual filtering to remove the numerous false-positives, and subsequent smoothing to obtain corelines that align well with the flow. In the space-time view, a LIC slice shows the respective vector field in which the critical points were extracted. The LIC slice is placed at the last time slice, which is also displayed separately below with unfiltered vortex cores. It is apparent that our method produces a much cleaner vector field, than  $v - f$ , and thus, critical point extraction is more stable. Note that smoothing  $f$  prior to subtraction is still far from the quality of our approach.

The BOUSSINESQ flow contains an unsteady convection simulation that develops around a heated cylinder. The resampled vector field was provided by Tino Weinkauf. Here, vortex movement is more complicated, see Fig. 7a for a space-time visualization of vortex corelines. Since vortices move rather slowly, Galilean invariance works well. Directly behind the obstacle, however, our method in Fig. 7b performs better than the Galilean invariant method of Weinkauf et al. [2007] in Fig. 7c, since we do not miss vortex corelines.

## 7.5 Objective Region-based Methods in 2D Flow

The importance of the reference frame is demonstrated in Fig. 8, cf. [Haller 2005]. Here, a steady saddle  $v(x, y) = (y + \frac{1}{1000}y^3, x + \frac{1}{1000}x^3)$  is observed in a steady and in a rotating reference frame with angular velocity equal two. In the steady frame in Fig. 8a,  $\lambda_2$  is non-negative, which correctly indicates no vortical behavior ( $\lambda_2 \approx 1$ ), whereas it clearly shows the presence of a vortex in the rotating frame ( $\lambda_2 \approx -3$ ) in Fig. 8b. Our objective method in Fig. 8c is invariant under rotations of the observer and even recovers the correct value range ( $\lambda_2 \approx 1$ ).

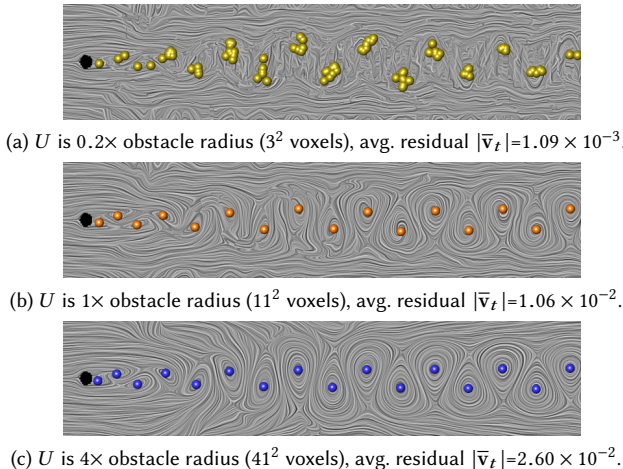


Fig. 10. 2D CYLINDER flow. From Figs. (a)-(c) the size of  $U$  increases. The larger  $U$ , the more stable is the reconstructed reference frame. The location of critical points (vortex centers) is almost identical for (b) and (c).

To define a vortex region, vorticity requires a threshold to be set, which can be problematic. Consider the flow from Section 7.2. The reference frame rotation in CCW direction amplifies CCW-rotating vortices and damps CW-rotating ones. Thus, the absolute vorticity of CW and CCW-rotating vortices differs in rotating frames, even though the vortices actually rotate with the same speed, but in different directions. In Fig. 9a, all vortices even exhibit a negative vorticity, incorrectly indicating four CCW rotating vortices. The value range of instantaneous vorticity deviation (IVD) in Fig. 9b depends on the neighborhood  $U(t)$ , in which vorticity was averaged. The smaller the area, the smaller the value range. Since our method removes the rotating frame, the absolute vorticity of the four vortices is the same as in the steady frame, see Fig. 9c. In this flow, the average of vorticity over the entire domain ( $U(t) = D$ ) results with IVD in the correct vorticity, as well, since all four vortices cancel out due to symmetry. This, however, is not generally the case.

## 7.6 Parameter: Neighborhood Size $U$

Our single parameter is the size of region  $U$ . We show results of varying window sizes in Fig. 10 for the 2D CYLINDER sequence. If  $U$  is chosen too small, the reconstructed frame is affected by noise, see Fig. 10a. Previous methods use topological simplification [Bujack et al. 2016; Kasten et al. 2016] to handle noisy extraction results. Our method gains stability by increasing the window size, being therefore less reliant on post-processing. Ideally, region  $U$  should have the expected vortex size. While the spatial stability of the reconstructed reference frame increases from Figs. 10b–10c with increasing  $U$ , the location of the vortex cores stayed nearly identical.

## 7.7 Objective Line-based Methods in 3D Flows

The TILTED VORTEX flow in Fig. 11 contains a 3D extension of the HELIX flow from Section 7.3. This time, the vortex is time-dependently tilted, while it rotates around a 3D axis. With our method, pathlines connect corelines that were extracted in different time steps, which is characteristic for a vortex. Galilean invariance is insufficient.

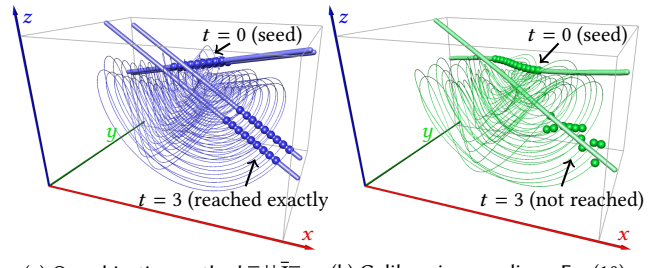


Fig. 11. In the 3D TILTED VORTEX, our method (a) extracts correct vortex corelines in contrast to the Galilean invariant method (b) of Weinkauf et al. [2007]. Seed points and end points of pathlines are highlighted by spheres, demonstrating that with our method, pathlines stay on corelines as desired.

Next, we compare our coreline extraction method in Fig. 12a with the approach of Weinkauf et al. [2007] in Fig. 12b. Even though, the SQUARE CYLINDER flow is a perfect candidate for Galilean invariant methods, our technique delivers corelines that are temporally more stable and it requires far less filtering effort to remove false-positives. We refer to the video for an animation.

## 7.8 Objective Region-based Methods in 3D Flow

In the literature, several objective region-based methods have been proposed for unsteady 3D flows. We test these methods in the SQUARE CYLINDER sequence, which was simulated by Camarri et al. [2005] and was kindly provided by Tino Weinkauf. In this flow, vortices form behind an obstacle and then move on a linear path downstream, resulting in a von-Kármán vortex street. Due to the almost constant equal-speed movement of the vortices, Galilean invariant techniques produce very good results. Any objective measure should be able to reveal vortex structures similarly well.

Fig. 13a shows IVD of Haller et al. [2016], which calculates vorticity relative to a neighborhood region. The magnitude range of this measure depends on the neighborhood size, and is thus not an absolute measure for vortex strength. When adjusting the transfer function, vortex patterns can be revealed well. Fig. 13b depicts LAVD of Haller et al. [2016], which accumulates IVD along particle trajectories and stores the result at the seed point. Particles that were released directly in front of the obstacle, flow around it and get trapped behind the obstacle in a regime with high vorticity, resulting in a LAVD response in front of the obstacle. We compute vorticity in an optimal reference frame, see Fig. 13c. Compared to IVD in Fig. 13a, we obtain (with the right transfer function for IVD) very similar results, but our method preserves the absolute magnitude range, making vorticity strength comparable across data sets. In the optimal reference frame, we can calculate other standard vortex measures objectively, such as  $\lambda_2$  in Fig. 13d, which gives very good results that are consistent with standard Galilean invariant  $\lambda_2$ . An earlier Lagrangian measure by Haller [2005] estimates the time a particle resides in non-hyperbolic regions and is visualized in Fig. 13e. While vortex areas are dominated by particles that stay coherently inside a non-hyperbolic region, the non-hyperbolic regions are not only limited to vortices, which results in several false-positives that might be difficult to filter. Finally, Fig. 13f illustrates  $\lambda_2$  that was

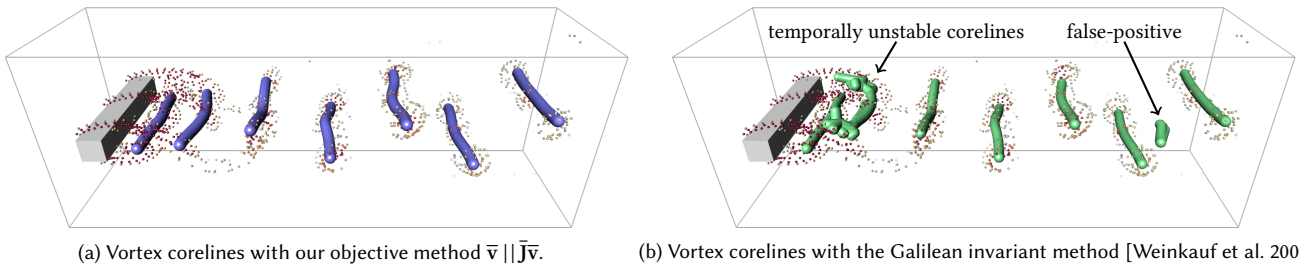


Fig. 12. In the SQUARE CYLINDER flow, our method extracts the vortex corelines more robustly than the Galilean invariant method of Weinkauf et al. [2007]. The latter is unstable directly in the wake of the cylinder, where corelines tend to bend slightly, which causes flickering. Occasionally, their method produces false-positives downstream. As a reference, particles are shown in both images in areas of high vorticity.

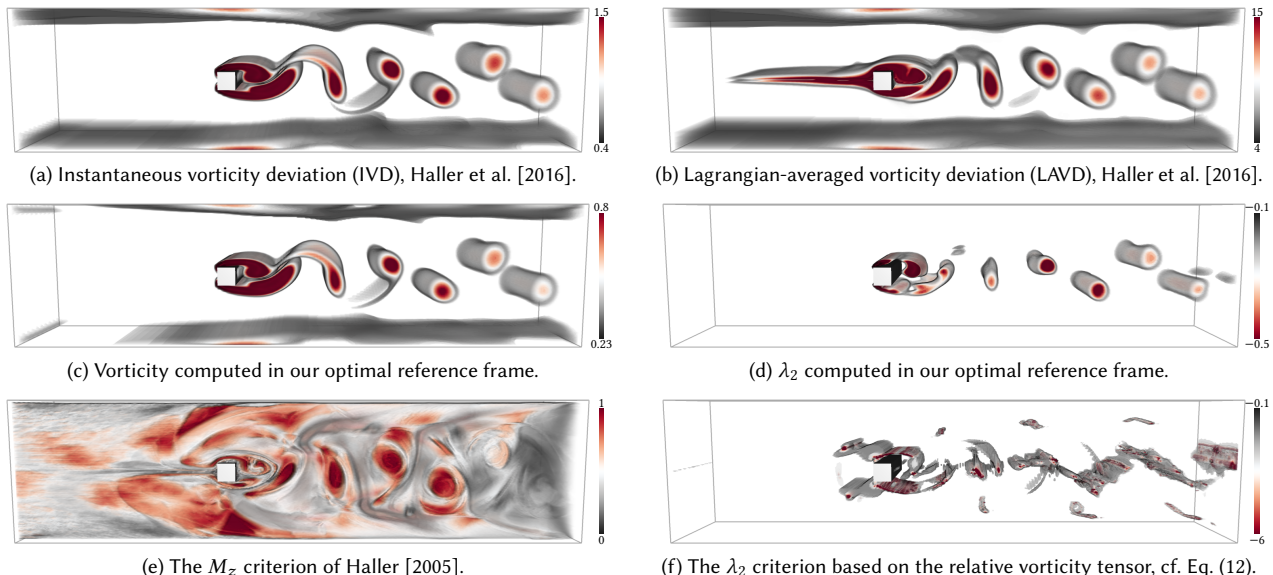


Fig. 13. In the SQUARE CYLINDER flow, objective region-based measures should be similar to traditional Galilean invariant measures. IVD (a), LAVD (b), our vorticity (c) and our  $\lambda_2$  (d) in optimal reference frames detect the von Kármán vortex street very well.  $M_z$  (e) produces false-positives and  $\lambda_2$  based on the relative vorticity tensor (f) is not consistent with traditional  $\lambda_2$ .

computed from the relative vorticity tensor, see Eq. (12). This measure produces false-positives and is not consistent with standard  $\lambda_2$ . In comparison, our objective  $\bar{\lambda}_2$  in Eq. (25) is the only objective counterpart to traditional  $\lambda_2$  that is consistent when vortices perform Galilean transformations. In summary, our objective vorticity and  $\lambda_2$  counterparts, as well as IVD and LAVD performed well. Note, however, that the last two are relative measures.

The ROTATING MIXER flow in Fig. 14 is a numerically-simulated flow with a bulk rotation that is stirred by three rotating paddles in a cylindrical container. In a motionless reference frame, small-scale vortices are not seen due to the bulk rotation. In our optimal frame, small-scale vortices are recovered, since the ambient rotation is coherent over finite regions  $U$ . Examples are shown in two close-ups, including vortices between the rotor blades and vortices that wind around the primary vortices, detaching from the blade tips.

## 7.9 Performance

We measured the performance of calculating  $\bar{v}$  and its derivatives on an Intel Core i7-6700HQ CPU with 16 GB RAM, and report the

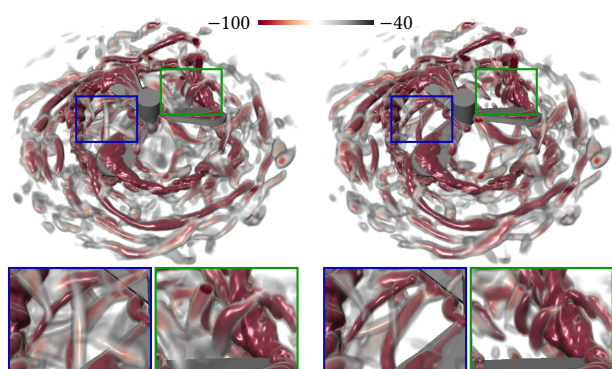
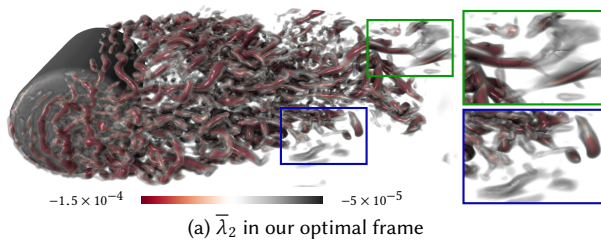


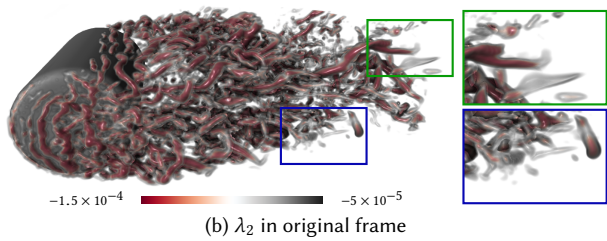
Fig. 14. Comparison of  $\bar{\lambda}_2$  and  $\lambda_2$  in the ROTATING MIXER flow. Dominant vortices are found with both methods. Our method reveals additional subtle details, such as weak tendrils between blades (blue) and vortices that wind around the strong wake vortex that is attached to the blade tip (green).

Data Set	Figure	Grid Resolution	Region $U$ (in voxels)	$\mathbf{M}^T \mathbf{M}$	Sum up $\hat{\mathbf{M}}, \hat{\mathbf{y}}$	Solve $\hat{\mathbf{M}}\mathbf{u} = \hat{\mathbf{y}}$	Compute $\bar{\mathbf{v}}, \bar{\mathbf{J}}, \bar{\mathbf{v}}_t, \bar{\mathbf{a}}$	Total time	Residual $ \bar{\mathbf{v}}_t $
ROTATING SADDLE	Fig. 8	$64 \times 64 \times 64$	$3^2$	1.21	0.04	<b>1.92</b>	0.19	3.36	$1 \times 10^{-5}$
STUART VORTEX	Fig. 3	$256 \times 128 \times 256$	$3^2$	4.71	0.24	<b>7.30</b>	0.80	13.05	$1 \times 10^{-9}$
FOUR CENTERS	Figs. 4,9	$128 \times 128 \times 128$	$7^2$	1.37	0.06	<b>1.86</b>	0.55	3.84	$6 \times 10^{-5}$
HELIX	Fig. 5	$128 \times 128 \times 512$	$7^2$	4.45	0.30	<b>7.40</b>	0.81	12.96	$6 \times 10^{-7}$
2D CYLINDER	Figs. 6,10	$640 \times 80 \times 1501$	$41^2$	55.93	1.80	<b>66.03</b>	12.78	136.54	$2 \times 10^{-2}$
BOUSSINESQ	Fig. 7	$100 \times 300 \times 1601$	$11^2$	29.00	1.61	<b>42.83</b>	8.63	82.07	$2 \times 10^{-2}$
SQUARE CYLINDER	Figs. 13,12	$400 \times 200 \times 50$	$41^3$	8.26	8.71	<b>14.50</b>	3.53	35.0	$8 \times 10^{-3}$
ROTATING MIXER	Fig. 14	$128 \times 128 \times 128$	$51^3$	0.99	0.80	<b>4.76</b>	0.88	7.43	$5 \times 10^{-2}$
TILTED VORTEX	Fig. 11	$128 \times 128 \times 128$	$11^3$	1.86	0.84	<b>4.99</b>	0.99	8.68	$2 \times 10^{-7}$
WALL-MOUNTED	Fig. 15	$256 \times 128 \times 128$	$21^3$	4.73	2.07	<b>10.34</b>	0.79	17.93	$3 \times 10^{-4}$

Table 1. Grid resolution, size of region  $U$  and performance (in secs.) for all data sets used throughout the paper; the bottleneck is printed **bold**. The last column lists the average residual of our optimization. For 2D data, we list numbers for all time steps, in 3D only a single time step is listed.



(a)  $\bar{\lambda}_2$  in our optimal frame



(b)  $\lambda_2$  in original frame

Fig. 15.  $\bar{\lambda}_2$  and  $\lambda_2$  in the WALL-MOUNTED CYLINDER flow. Dominant vortices are found with both methods. Our method shows further subtle effects downstream. In turbulent flow, there is no distinguished reference frame, in which an entire finite region  $U$  appears steady.



Fig. 16. Direct visualization of our smooth reference frame motion direction  $\tilde{\mathbf{v}} = \bar{\mathbf{v}} - \mathbf{v}$  compared to  $\mathbf{f}$  in the BOUSSINESQ flow.

grid resolution, neighborhood size  $U$ , timings and average residuals in Table 1. We performed the computations on regular grids, for which the computation time scales linearly with the number of grid points. With summed-area tables, the entire computation is in  $O(n)$  even for large neighborhood sizes  $U$ . For 2D data, we list the time for all time steps and for 3D, we list a single time step. The pipeline steps of Section 6 are listed individually and the bottleneck is printed bold, which was in all cases the solution of  $\hat{\mathbf{M}}\mathbf{u} = \hat{\mathbf{y}}$ . The total time ranges from a few seconds to roughly two minutes, which is acceptable for a one-time precomputation. For unsteady fields that were constructed by transformation of a steady flow, the residual is close to zero. In turbulent regimes or when vortices deform, the residual grows for larger  $U$ , since then, the temporal evolution is not governed by rotation and translation only.

## 7.10 Discussion

**Turbulence.** In unsteady flows, there is no local frame, in which the flow performs a coherent motion in a finite neighborhood  $U$ . An example of this is given by the turbulent WALL-MOUNTED CYLINDER flow in Fig. 15. In the turbulent wake of the cylinder, particles move almost randomly. Our method only finds a frame that is in a least-squares sense as steady as possible. In this example, it does not detect more or less vortical behavior. We do, however, find further hints of vortical behavior downstream in less-turbulent areas.

**Vector Field Decomposition.** Our method can be seen as a local vector field decomposition of a flow  $\mathbf{v}$  into two parts:

$$\mathbf{v} = \bar{\mathbf{v}} + \tilde{\mathbf{v}} \quad \text{with} \quad \tilde{\mathbf{v}} = -sk(\bar{\mathbf{u}}_1)\mathbf{x} - \bar{\mathbf{u}}_2 \quad (30)$$

which follows from rearranging Eq. (20). Thereby,  $\bar{\mathbf{v}}$  is as steady as possible and  $\tilde{\mathbf{v}}$  contains all remaining information about the reference frame transformation. The linear vector field  $\tilde{\mathbf{v}}$  is divergence-free, since its Jacobian is skew-symmetric, cf. Eq. (1). To illustrate the reference frame movement, we visualize  $\tilde{\mathbf{v}}$  in Fig. 16.

**Divergence and Curl.** When using  $\bar{\mathbf{J}}$ , the transformation into the optimal reference frame preserves divergence, but not curl:

$$\nabla \cdot \bar{\mathbf{v}} = \nabla \cdot \mathbf{v} \quad \text{and} \quad \nabla \times \bar{\mathbf{v}} \neq \nabla \times \mathbf{v} \quad (31)$$

The divergence is preserved since  $\bar{\mathbf{v}}$  is computed in Eq. (20) by subtracting the linear divergence-free vector field  $\tilde{\mathbf{v}} = -sk(\bar{\mathbf{u}}_1)\mathbf{x} - \bar{\mathbf{u}}_2$  in Eq. (30) from  $\mathbf{v}$ . Curl is generally not preserved, which is desired and necessary to remove rotations for example in Fig. 8. Unlike divergence, curl cannot be preserved as it is not objective.

**Derivatives in Local Reference Frames.** We compute the optimal reference frame locally in space and time for each point *individually*. Thereby, the transformation  $\mathbf{Q}, \mathbf{c}$  is assumed to be spatially-constant and temporally-varying. Since the points in the domain are treated independently, there is no continuity in  $\mathbf{Q}$  and  $\mathbf{c}$  enforced among neighboring voxels in the domain. As a result, neither spatial nor temporal derivatives of  $\bar{\mathbf{v}}, \mathbf{Q}$  and  $\mathbf{c}$  can be computed via finite differences. For this reason, we solve for  $\mathbf{Q}, \dot{\mathbf{Q}}, \ddot{\mathbf{Q}}$  and  $\mathbf{c}, \dot{\mathbf{c}}, \ddot{\mathbf{c}}$  separately, and derived the equations for  $\bar{\mathbf{J}}, \bar{\mathbf{a}}, \bar{\mathbf{v}}_t$  in Eqs. (21)–(23), which have to be applied when computing vortex measures as in Section 5. Fig. 17 demonstrates the error introduced by finite differences. In the future, it is imaginable to not treat each point individually and to include spatial derivatives in  $\mathbf{Q}$  when computing the optimal frame. Then, explicit formulas for  $\bar{\mathbf{J}}$  and  $\bar{\mathbf{a}}$  might no longer be needed.

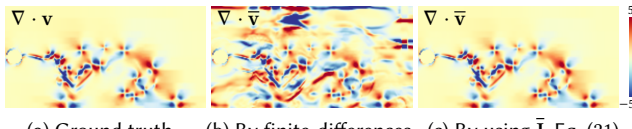


Fig. 17. Since we fit optimal frames for each point individually,  $\bar{J}$  in Eq. (21) must be used to compute derivatives. We show for the Boussinesq flow that  $\nabla \cdot \mathbf{v} = \nabla \cdot \bar{\mathbf{v}}$ , with  $U = 21^2$ . Finite-differences lead to the wrong result.

*Existence of Minimum.* Note that  $\hat{\mathbf{M}}$  is not invertible if  $\mathbf{v}$  is linear or rotationally-symmetric. In these cases, a neighborhood  $U$  does not provide enough information for a unique optimal frame, no matter how large  $U$  is, which is why we added cubic terms in Fig. 8. Other techniques such as FTLE similarly do not work in linear fields. In practice, we did not observe a singular  $\hat{\mathbf{M}}$  in numerical flows. In the future, we would like to search for other *objective* regularizers, aside from increasing  $U$ , to eliminate this theoretical limitation.

*Limit Observations.* In contrast to IVD of Haller et al. [2016] our method can be studied in the limit of vanishing neighborhood  $U$ . In Appendix C, we provide a truly local approach to compute  $\bar{\mathbf{v}}$ ,  $\bar{\mathbf{J}}$ ,  $\bar{\mathbf{a}}$  and  $\bar{\mathbf{v}}_t$  by collapsing region  $U$  to a point. In practice, the approach is less relevant, since it involves third-order derivatives.

*Other Distinguished Reference Frames.* Our method is objective, since it selects for any rotating and translating reference frame of  $\mathbf{v}$  the same distinguished optimal frame and applies all vortex measures there. Note that any other “special” reference frame that could be selected from all possible choices would also be objective.

*Repeated Application.* Applying our method twice does not change the result, regardless of whether  $U$  is local or spans the entire domain. If  $U$  is local, however, the vectors in the neighborhood must be transformed into a common reference frame—it does not matter which one—before  $\mathbf{M}^T \mathbf{M}$  and  $\mathbf{M}^T \mathbf{v}_t$  are calculated and integrated, since otherwise the method would fit an optimal frame to vectors that currently reside in different frames, which produces artifacts.

*Higher-Order Methods.* Our examples demonstrated first-order vortex extractors, such as  $\lambda_2$ , vorticity and Sujudi-Haines. It shall be noted that all higher-order methods, e.g., Roth and Peikert [1998], that use second-order derivatives or higher, can be made objective, as well, since all spatial derivatives of  $\bar{\mathbf{v}}$  are objective.

*Objective Lagrangian Vortex Measures.* All objective Eulerian measures, such as  $\lambda_2$  and  $\bar{\omega}$ , can be extended to Lagrangian measures for stability by computing the vortex measures using  $\bar{\mathbf{v}}$ ,  $\bar{\mathbf{J}}$ ,  $\bar{\mathbf{a}}$  and  $\bar{\mathbf{v}}_t$ , and integrating them along pathlines in the original field  $\mathbf{v}$ .

## 8 CONCLUSION

In this paper, we proposed a general approach to transform an unsteady vector field into a reference frame, in which the flow locally appears as steady as possible, i.e., in which the temporal derivative of the flow vanishes. We rephrased the transformed temporal derivative to separate the parameters of the optimal reference transformation from local differential flow properties, which allowed us to linearly solve for the optimal transformation in a local neighborhood. In the optimal reference frame, standard vortex extraction

techniques that are based on velocity and its derivatives become objective. Therefore, their extraction finally becomes independent of the choice of the reference frame. We experimented with objective versions of  $\lambda_2$ , vorticity and Sujudi-Haines. In the future, we would like to apply our method to other vortex extraction techniques.

## A PROOF OF EQUATIONS (4)–(9)

Considering a particle trajectory  $\mathbf{x}(t)$  with velocity  $\dot{\mathbf{x}} = \frac{d\mathbf{x}}{dt}$  and acceleration  $\ddot{\mathbf{x}} = \frac{d\dot{\mathbf{x}}}{dt}$ , Eq. (3) transforms velocity and acceleration to

$$\dot{\mathbf{x}}^* = \underline{\mathbf{Q}} \dot{\mathbf{x}} + \dot{\underline{\mathbf{Q}}} \mathbf{x} + \dot{\mathbf{c}} \quad (32)$$

$$\ddot{\mathbf{x}}^* = \underline{\mathbf{Q}} \ddot{\mathbf{x}} + 2\dot{\underline{\mathbf{Q}}} \dot{\mathbf{x}} + \ddot{\underline{\mathbf{Q}}} \mathbf{x} + \ddot{\mathbf{c}}. \quad (33)$$

Assuming the trajectory  $\mathbf{x}(t)$  as pathline of the velocity field  $\mathbf{v}(\mathbf{x}, t)$  gives the differential equations

$$\dot{\mathbf{x}} = \mathbf{v}(\mathbf{x}, t) \quad \ddot{\mathbf{x}} = \mathbf{a}(\mathbf{x}, t) \quad (34)$$

Inserting  $\dot{\mathbf{x}}$  into (32) gives Eq. (4) and inserting  $\ddot{\mathbf{x}}$  into (33) gives Eq. (6). Eq. (5) is obtained from the partial derivatives of Eq. (4) as  $\mathbf{J}^* = (\mathbf{v}_x^*, \mathbf{v}_y^*, \mathbf{v}_z^*)$ . Eq. (7) follows from (4)–(6) and  $\mathbf{v}_t^* = \mathbf{a}^* - \mathbf{J}^* \mathbf{v}^*$ . Eq. (8) follows from  $\mathbf{J} = \mathbf{S} + \Omega$ , (5) and the fact that  $\dot{\underline{\mathbf{Q}}} \underline{\mathbf{Q}}^T$  is a skew-symmetric tensor, i.e.,  $\dot{\underline{\mathbf{Q}}} \underline{\mathbf{Q}}^T = -(\dot{\underline{\mathbf{Q}}} \underline{\mathbf{Q}}^T)^T$ . Eq. (9) follows from Eqs. (2) and (5).

## B PROOF THAT $\bar{\mathbf{v}}, \bar{\mathbf{J}}, \bar{\mathbf{v}}_t, \bar{\mathbf{a}}$ ARE OBJECTIVE

Let  $\mathbf{w}$  be the observation of  $\mathbf{v}$  under an arbitrary frame  $(\mathbf{R}, \mathbf{d})$ , where  $\mathbf{R}$  is an arbitrary rotation matrix and  $\mathbf{d}$  is a translation vector. Further, let  $\bar{\mathbf{w}}$  be the observation of  $\mathbf{w}$  under its optimal frame  $(\underline{\mathbf{Q}}, \underline{\mathbf{c}})$ . To show the objectivity of  $\bar{\mathbf{v}}$ , we follow Definition 2.1 and show that the optimal frames of  $\mathbf{v}$  and  $\mathbf{w}$  are related by:

$$\bar{\mathbf{w}} = \mathbf{R} \bar{\mathbf{v}} \quad (35)$$

To find  $\bar{\mathbf{w}}$ , we search for its optimal frame  $(\underline{\mathbf{Q}}, \underline{\mathbf{c}})$  that minimizes

$$\int_{\mathbf{R}U+\mathbf{d}} \|\mathbf{w}_t^*\|^2 dV \rightarrow \min. \quad (36)$$

From the perspective of  $\mathbf{v}$ , the optimal frame of  $\mathbf{w}$  is reached by the transformation:  $\mathbf{x}^* = \underline{\mathbf{Q}}(\mathbf{R}\mathbf{x} + \mathbf{d}) + \underline{\mathbf{c}}$ . Thus,  $\mathbf{w}_t^*$  can be expressed from the perspective of  $\mathbf{v}$ , which allows us to use  $\mathbf{v}_t$ :

$$\mathbf{w}_t^* = \underline{\mathbf{Q}}(\mathbf{v}_t - \mathbf{M} \mathbf{u}) \quad (37)$$

where  $\mathbf{x}^* = \underline{\mathbf{Q}} \mathbf{x} + \underline{\mathbf{c}}$  with  $\underline{\mathbf{Q}} = \mathbf{Q} \mathbf{R}$ ,  $\underline{\mathbf{c}} = \mathbf{Q} \mathbf{d} + \underline{\mathbf{c}}$ , and

$$\underline{\mathbf{u}} = \begin{pmatrix} ap(\underline{\mathbf{Q}}^T \dot{\underline{\mathbf{Q}}}) \\ \underline{\mathbf{Q}}^T \dot{\underline{\mathbf{c}}} \\ ap(\underline{\mathbf{Q}}^T \dot{\underline{\mathbf{Q}}} - (\underline{\mathbf{Q}}^T \dot{\underline{\mathbf{Q}}})^2) \\ -(\underline{\mathbf{Q}}^T \dot{\underline{\mathbf{c}}} - \underline{\mathbf{Q}}^T \dot{\underline{\mathbf{Q}}} \underline{\mathbf{Q}}^T \dot{\underline{\mathbf{c}}}) \end{pmatrix}. \quad (38)$$

Since  $\underline{\mathbf{Q}}$  and  $\mathbf{Q}$  are rotations that do not change the length of  $\mathbf{w}_t^*$  and  $\mathbf{v}_t^*$  in Eqs. (14) and (37), we can see that  $\underline{\mathbf{u}}$  minimizing (36) and  $\bar{\mathbf{u}}$  minimizing (13) are identical. Given the parameters  $\bar{\mathbf{u}} = \underline{\mathbf{u}}$ , we compute  $\bar{\mathbf{v}}$  and  $\bar{\mathbf{w}}$  in the optimal reference frame:

$$\bar{\mathbf{v}} = \mathbf{Q}(\mathbf{v} + sk(\bar{\mathbf{u}}_1) \mathbf{x} + \bar{\mathbf{u}}_2) \quad (39)$$

$$\bar{\mathbf{w}} = \underline{\mathbf{Q}}(\mathbf{v} + sk(\bar{\mathbf{u}}_1) \mathbf{x} + \bar{\mathbf{u}}_2) \quad (40)$$

and from this we get for  $\mathbf{Q} = \mathbf{I}$  that  $\bar{\mathbf{w}} = \mathbf{R} \bar{\mathbf{v}}$ , i.e., Eq. (35). The objectivity of  $\bar{\mathbf{J}}, \bar{\mathbf{v}}_t, \bar{\mathbf{a}}$  is shown in a similar way.

### C LOCAL VERSION WITHOUT NEIGHBORHOOD

Up to now, our approach depends on the choice of the region  $U$  at each point. We provide a truly local version by collapsing  $U$  to a point. For this, Eq. (13) is replaced by

$$\begin{aligned} & \|v_t^*\|^2 + \|v_{xt}^*\|^2 + \|v_{yt}^*\|^2 + \|v_{zt}^*\|^2 \\ & + \varepsilon^2 (\|v_{xyt}^*\|^2 + \|v_{yzt}^*\|^2 + \|v_{xzt}^*\|^2) \rightarrow \min. \end{aligned} \quad (41)$$

where  $\varepsilon$  is a small value responsible for a regularization of the system. Note that for divergence-free flows, Eq. (41) with  $\varepsilon = 0$  does not provide enough information to find a unique minimum. From Eq. (41), we get the system in Eq. (18) with

$$\begin{aligned} \hat{\mathbf{M}} &= \mathbf{M}^T \mathbf{M} + \mathbf{M}_x^T \mathbf{M}_x + \mathbf{M}_y^T \mathbf{M}_y + \mathbf{M}_z^T \mathbf{M}_z \\ &+ \varepsilon^2 (\mathbf{M}_{xy}^T \mathbf{M}_{xy} + \mathbf{M}_{xz}^T \mathbf{M}_{xz} + \mathbf{M}_{yz}^T \mathbf{M}_{yz}) \end{aligned} \quad (42)$$

$$\begin{aligned} \hat{\mathbf{y}} &= \mathbf{M}^T \mathbf{v}_t + \mathbf{M}_x^T \mathbf{v}_{xt} + \mathbf{M}_y^T \mathbf{v}_{yt} + \mathbf{M}_z^T \mathbf{v}_{zt} \\ &+ \varepsilon^2 (\mathbf{M}_{xy}^T \mathbf{v}_{xyt} + \mathbf{M}_{xz}^T \mathbf{v}_{xzt} + \mathbf{M}_{yz}^T \mathbf{v}_{yzt}). \end{aligned} \quad (43)$$

Note that for  $\varepsilon \neq 0$ , Eqs. (42) and (43) contain third-order derivatives of  $\mathbf{v}$ , implying a limited numerical stability of the method. The image in Fig. 3a was computed with this approach. The timings in Table 1 refer to the non-local version, which gives the same result.

### REFERENCES

- Gianni Astarita. 1979. Objective and generally applicable criteria for flow classification. *Journal of Non-Newtonian Fluid Mechanics* 6, 1 (1979), 69–76.
- Dirk Bauer and Ronald Peikert. 2002. Vortex Tracking in Scale-space. In *Proc. Symposium on Data Visualisation*. 233–240.
- H. Bhatia, G. Norgard, V. Pascucci, and Peer-Timo Bremer. 2013. The Helmholtz-Hodge Decomposition—A Survey. *IEEE Transactions on Visualization and Computer Graphics* 19, 8 (2013), 1386–1404.
- Harsh Bhatia, Valerio Pascucci, Robert M. Kirby, and Peer-Timo Bremer. 2014. Extracting Features from Time-Dependent Vector Fields Using Internal Reference Frames. *Computer Graphics Forum (Proc. EuroVis)* 33, 3 (2014), 21–30.
- R. Bujack, M. Hlawitschka, and K. I. Joy. 2016. Topology-inspired Galilean invariant vector field analysis. In *IEEE Pacific Visualization Symposium*. 72–79. DOI: <https://doi.org/10.1109/PACIFICVIS.2016.7465253>
- S. Camarri, M.-V. Salvetti, M. Buffoni, and A. Iollo. 2005. Simulation of the three-dimensional flow around a square cylinder between parallel walls at moderate Reynolds numbers. In *XVII Congresso di Meccanica Teorica ed Applicata*.
- R Drouot and M Lucius. 1976. Approximation du second ordre de la loi de comportement des fluides simples. Lois classiques déduites de la Zintroduction à un nouveau tenseur objectif. *Archivum Mechaniki Stosowanej* 28, 2 (1976), 189–198.
- T. Günther, Maik Schulze, and H. Theisel. 2016. Rotation Invariant Vortices for Flow Visualization. *IEEE Transactions on Visualization and Computer Graphics (Proc. IEEE SciVis 2015)* 22, 1 (2016), 817–826.
- T. Günther and H. Theisel. 2014. Vortex Cores of Inertial Particles. *IEEE Transactions on Visualization and Computer Graphics (Proc. IEEE SciVis)* 20, 12 (2014), 2535–2544.
- G. Haller. 2005. An objective definition of a vortex. *Journal of Fluid Mechanics* 525 (2005), 1–26.
- George Haller. 2015. Lagrangian coherent structures. *Annual Review of Fluid Mechanics* 47 (2015), 137–162.
- George Haller, Alireza Hadjighasem, Mohammad Farazmand, and Florian Huhn. 2016. Defining coherent vortices objectively from the vorticity. *Journal of Fluid Mechanics* 795 (2016), 136–173.
- J. C. R. Hunt. 1987. Vorticity and vortex dynamics in complex turbulent flows. *Transactions on Canadian Society for Mechanical Engineering (Proc. CANCAM)* 11, 1 (1987), 21–35.
- Jinhee Jeong and Fazle Hussain. 1995. On the identification of a vortex. *Journal of Fluid Mechanics* 285 (1995), 69–94.
- Jens Kasten, Ingrid Hotz, Bernd R. Noack, and Hans-Christian Hege. 2011a. On the Extraction of Long-living Features in Unsteady Fluid Flows. In *Topological Methods in Data Analysis and Visualization*. 115 – 126.
- Jens Kasten, Jan Reininghaus, Ingrid Hotz, and Hans-Christian Hege. 2011b. Two-Dimensional Time-Dependent Vortex Regions Based on the Acceleration Magnitude. *IEEE Transactions on Visualization and Computer Graphics (Proc. IEEE SciVis)* 17, 12 (2011), 2080–2087.
- J. Kasten, J. Reininghaus, Hotz I., H.-C. Hege, B. R. Noack, G. Daviller, and M. Morzynski. 2016. Acceleration feature points of unsteady shear flows. *Archives of Mechanics* 68, 1 (2016), to appear.
- Roberts S. Laramee, Helwig Hauser, Lingxiao Zhao, and Frits H. Post. 2007. Topology-Based Flow Visualization, The State of the Art. In *Topology-based Methods in Visualization*. Springer Berlin Heidelberg, 1–19. DOI: [https://doi.org/10.1007/978-3-540-70823-0\\_1](https://doi.org/10.1007/978-3-540-70823-0_1)
- Hans J. Lugt. 1979. The dilemma of defining a vortex. In *Recent developments in theoretical and experimental fluid mechanics*. Springer, 309–321.
- R. S. Martins, A. S. Pereira, G. Mompean, L. Thais, and R. L. Thompson. 2016. An objective perspective for classic flow classification criteria. *Comptes Rendus Mécanique* 344 (Jan. 2016), 52–59. DOI: <https://doi.org/10.1016/j.crme.2015.08.002> arXiv:physics.fl-dyn/1506.03384
- Akira Okubo. 1970. Horizontal dispersion of floatable particles in the vicinity of velocity singularities such as convergences. *Deep Sea Research and Oceanographic Abstracts* 17, 3 (1970), 445–454.
- Ronald Peikert and Martin Roth. 1999. The “Parallel Vectors” Operator – A Vector Field Visualization Primitive. In *Proc. IEEE Visualization*. 263–270.
- A. E. Perry and M. S. Chong. 1994. Topology of Flow Patterns in Vortex Motions and Turbulence. *Applied Scientific Research* 53, 3 (1994), 357–374. DOI: <https://doi.org/10.1007/BF00849110>
- Stéphane Popinet. 2004. Free computational fluid dynamics. *Cluster World* 2 (2004).
- Frits H. Post, Benjamin Vrolijk, Helwig Hauser, Robert S. Laramee, and Helmut Doleisch. 2003. The State of the Art in Flow Visualisation: Feature Extraction and Tracking. *Computer Graphics Forum* 22, 4 (2003), 775–792. DOI: <https://doi.org/10.1111/j.1467-8659.2003.00723.x>
- Martin Roth and Ronald Peikert. 1998. A higher-order method for finding vortex core lines. In *Proc. IEEE Visualization*. 143–150.
- J. Sahner, T. Weinkauf, and H.-C. Hege. 2005. Galilean Invariant Extraction and Iconic Representation of Vortex Core Lines. In *Proc. EuroVis*. 151–160.
- J. Sahner, T. Weinkauf, N. Teuber, and H.-C. Hege. 2007. Vortex and Strain Skeletons in Eulerian and Lagrangian Frames. *IEEE Trans. Vis. and Computer Graphics* 13, 5 (2007), 980–990.
- T. Schafhitzel, J. Vollrath, J. Gois, D. Weiskopf, A. Castelo, and T. Ertl. 2008. Topology-Preserving lambda2-based Vortex Core Line Detection for Flow Visualization. *Computer Graphics Forum (Proc. EuroVis)* 27, 3 (2008), 1023–1030.
- Mattia Serra and George Haller. 2016a. Forecasting Long-Lived Lagrangian Vortices from their Objective Eulerian Footprints. *J. Fluid Mech.* (2016), to appear.
- Mattia Serra and George Haller. 2016b. Objective Eulerian coherent structures. *Chaos: An Interdisciplinary Journal of Nonlinear Science* 26, 5 (2016), 053110.
- D. Sujudi and R. Haines. 1995. Identification of Swirling Flow in 3D Vector Fields. Technical Report. Departement of Aeronautics and Astronautics, MIT. AIAA Paper 95-1715.
- Michael Tabor and I. Klapper. 1994. Stretching and alignment in chaotic and turbulent flows. *Chaos, Solitons & Fractals* 4, 6 (1994), 1031–1055.
- H. Theisel, J. Sahner, T. Weinkauf, H.-C. Hege, and H.-P. Seidel. 2005. Extraction of parallel vector surfaces in 3D time-dependent fields and application to vortex core line tracking. In *Proc. IEEE Visualization*. 631–638.
- H. Theisel and H.-P. Seidel. 2003. Feature Flow Fields. In *Proc. Symposium on Data Visualisation*. 141–148.
- Roney L. Thompson. 2008. Some perspectives on the dynamic history of a material element. *International Journal of Engineering Science* 46, 3 (2008), 224–249.
- Yiying Tong, Santiago Lombeyda, Anil N. Hirani, and Mathieu Desbrun. 2003. Discrete Multiscale Vector Field Decomposition. *ACM Trans. Graph. (Proc. SIGGRAPH)* 22, 3 (2003), 445–452.
- Clifford Truesdell and Walter Noll. 1965. *The nonlinear field theories of mechanics*. Handbuch der Physik, Band III/3, e by Flügge, S., (ed.), Springer-Verlag, Berlin.
- T. Weinkauf, J. Sahner, H. Theisel, and H.-C. Hege. 2007. Cores of Swirling Particle Motion in Unsteady Flows. *IEEE Transactions on Visualization and Computer Graphics (Proc. Visualization)* 13, 6 (2007), 1759–1766.
- John Weiss. 1991. The dynamics of enstrophy transfer in two-dimensional hydrodynamics. *Physica D: Nonlinear Phenomena* 48, 2–3 (1991), 273–294.

Received February 2017; revised March 2017; final version June 2017; accepted July 2017